Supporting Information

Innovative ligand-assisted synthesis of NIR-activated iron oxide for cancer theranostics

Mei-Yi Liao,[1] Ping-Shan Lai,[2] Hsiu-Ping Yu,[2] Hong-Ping Lin*[1] and Chih-Chia Huang*[3]

[1]Department of Chemistry, National Cheng Kung University, Tainan 701, Taiwan
[2]Department of Chemistry, Center of Nanoscience and Nanotechnology, National Chung Hsing University, Taichung 402, Taiwan
[3]Biophotonics and Molecular Imaging Research Center (BMIRC), National Yang-Ming University, Taipei 112, Taiwan

[*]**Corresponding authors:**

E-mail: hplin@mail.ncku.edu.tw; cchuang-ym@ym.edu.tw,

Experiment Section

Materials. Iron(II) chloride tetrahydrate ($FeCl_2 \cdot 4H_2O$, 99–102 %) (Merck), sodium citrate (100 %, J. T. Baker), benzene-1,3,5-tri-carboxylic acid (trimesic acid (TMA), 98 %) (Alfa Aesar), Sodium hydroxide (NaOH, 99 %0 (Riedel-de Haën), γ-Fe_2O_3 nanoparticels (<50 nm, Aldrich), aminopropyl-triethoxysilane (APTES, 99%) (Acros), tetraethyl orthosilicate (TEOS, 98%) (Acros), and ethanol (EtOH, 99.9%, J.T. Baker) were purchased and used without further purification.

Preparation of optical-activated iron oxide nanostructure: 10 mL of $FeCl_2 \cdot 4H_2O$ (50 mM), 4.5 mL of TMA (25 mM), 18 mg of NaOH, and 0.15 g of sodium citrate were mixed by stirring and then immediately transferred to a 23-mL Teflon-lined stainless steel autoclave to be heated at 200 ^oC for 12 h. After reaction, the hydrothermal process was stopped by cooling the solution to room temperature to collect as-obtained colored precipitates by centrifugation. A centrifugation-washing process with deionized water was repeated three times to purify the as-synthesized iron oxide products

Preparation of optical-activated α-Fe_2O_3 nanostructure: Following the aforementioned synthesis with γ-Fe_2O_3 nanoparticels as the iron(III) source, 10 mL of water, including γ-Fe_2O_3 nanoparticels (0.345 mol), 4.5 mL of TMA (25 mM), 18 mg of NaOH, and 0.15 g of sodium citrate were mixed by stirring and then immediately transferred to a 23-mL Teflon-lined stainless steel autoclave to be heated at 200 ^oC for 24 h. Washing and purification processes were followed according to the above description.

Preparation of NIR-activated Fe_3O_4@$mSiO_2$ nanostructure: The mesoporous silica-coated Fe_3O_4 (Fe_3O_4@$mSiO_2$) nanostructure was synthesized following our previous reports[1,2] with a slight modification: 0.86 mL of Fe_3O_4 nanostructures (1800 $ppm_{[Fe]}$) after 12 h of hydrothermal reaction and purification was dispersed in 4.575 mL of CTAB (5.46 mM) and NaOH solution (1.37 mM) in a 20 mL glass vial. A continuous Ar flow was applied to the vial to eliminate air. Next, 0.026 mL of TEOS was added into the mixture under ultrasonic treatment in a sonication bath at 55℃. The reaction glass vial was enclosed with a foil-lined urea screw cap in the Ar environment. After 2 h of reaction time, the resulting black solution was collected using centrifugation and then washed 3 times with distilled water. Using APTES/ethanol extraction, the CTAB were removed from the mesoporous silica shells of Fe_3O_4@$mSiO_2$

nanostructures. 1.55 $mg_{[Fe]}$ of the Fe_3O_4@$mSiO_2$ nanostructures was then suspended in ethanol in sonication bath at 80 ^oC in the 20 mL glass vial with continuous Ar flow. Subsequently, 84 μL of APTES was added to yield APTES-functionalized Fe_3O_4@$mSiO_2$ nanostructures (named as NIR-activated nanocomposites). The reaction glass vial was enclosed with a foil-lined urea screw cap in the Ar environment. After the interaction (6 h) of mesoporous silica nanoshells with APTES molecules under ultrasonic treatment in the sonication bath at 80℃, the black product was collected by a centrifugation/re-suspension process for more than 3 times and washed with ethanol.

Temperature evolution at 808 nm laser irradiation: The temperature elevation of the NIR-activated nanocomposites was measured by placing the material solutions (400 $ppm_{[Fe]}$) in 96 well plates and irradiating them using a 808 nm continuous wave (CW) diode laser.[3] A thermalcouple was immersed in the material solutions to determine temperature. The CW laser had a power density of 2 W/cm^2.

Photothermal therapy of KB cancer cells: KB cancer cells were cultured in 96-well plates with MEM, 10% FBS and penicillin-streptomycin-neomycin and maintained in an incubator under a 5% CO_2 atmosphere at 37 °C. Each well contained 8×10^3 cells for a culture time of 24h. NIR-activated nanocomposites were added to the cells and incubated for 1 h at 37 ^oC. To wash away the unbound NIR-activated nanocomposites, the wells were rinsed with PBS buffer three times, and then a fresh RPMI medium was added to each well. The photothermal killing of cancer cells was performed by using a CW diode laser with a wavelength of 808 nm. After laser irradiation, another 24 h of incubation time was performed. Then, the cell viability was examined by using the MTT assays:[1-4] the original culture medium was removed and replaced with 100 μL of the new culture medium containing 10% MTT reagent. The cells were then incubated for 4 h at 37°C to allow formazan dye to form. The culture medium in each well was then removed, and dimethyl sulfoxide (DMSO) (200 μL/well) was added for an additional 10 min of incubation. After the cells had been centrifuged, the resulting formazan in each well was transferred to an ELISA plate. Quantification for determining cell viability was done using a scanning multiwell ELISA reader at 485 nm (SpectraMax® M2^e, Molecular Devices, USA).[4]

Measuring NIR-activated nanocomposites using confocal laser scanning microscopy. KB Cells were cultured in MEM at 37 °C supplied with 5% CO_2/95% air. Cells were trypsinized and seeded in 8-well chamber slides with 1.5×10^4 cells of each well. After 24 h of incubation, each well was washed twice with phosphate-buffered saline (PBS), and then 0.3 mL of NIR-activated nanocomposites (120 μg/mL in MEM) were added. After 2 h of incubation, the treated cells were washed with PBS and then fixed using 4% paraformaldehyde/PBS for 30 min at 37 °C. The cytoskeleton and nucleus were stained using Alexa 488 phalloidin (green) and DAPI (blue) for confocal laser scanning microscopy (CLSM) (Leica-SP5, Leica Microsystems Heidelberg GmbH, Heidelberg, Germany)

***In vitro* magnetic resonance imaging (MRI) assays:** The *in vitro* MR image contrast effect of the magnetite nanoparticles was evaluated using a Signa 3 T clinical MR system (GE Healthcare, USA). For T_2-weighted imaging, the NIR-activated nanocomposites with various concentration of iron were dispersed in a 0.5% agarose gel solution. The samples were placed in a homemade water tank positioned in the 8 channel head coil. A two-dimensional T_2-weighted fast-spin echo pulse sequence was applied (TR/TE=3017/98.9). The matrix size was 320×192, the field of view was 14×7 cm, the slice thickness was 1 mm with a 0.5 mm gap, and the total scan time was 2 minutes and 43 seconds at a NEX of two. The images were further analyzed at the image workstation provided by GE Healthcare (Advantage Workstation 4.207). The images were analysed by Image J provided by the NIH (http://rsbweb.nih.gov/ij/). The detail examinations of the proton relaxivities r_1 and r_2 related Fe_3O_4 strcuture and surface are complicated and will be reported further in the future.

***In vivo* examinations:** The *in vivo* experimental protocols were approved by the Institutional Animal Care and Use Committee of National Chung Hsing University (IACUC of NCHU). Female BALB/cAnN.Cg-*Foxn1*^{nu}/CrlNarl nude mice (4-5 weeks old, 20±2 g) were obtained from the National Laboratory Animal Center (Taiwan). All mice were kept in an air-conditioned facility fitted with an artificial light–dark cycle and were provided with standard food and filtered water. The mice were acclimated to this environment for at least three days prior to subcutaneous injection in the right hindquarter with 1×10^7 KB cells suspended in serum-free Minimum Essential Medium. The tumour

volume was calculated using the formula 1/2(4π/3)(L/2)(W/2)H, where L is the length, W is the width, and H is the height of the tumour. Treatments were initiated when the tumours reached a volume of 100 mm^3. The animals were injected with 0.1 ml of H_2O (control group) or NIR-activated nanocomposites (0.5 mg Fe/kg) via an intratumoral injection. The animals that received H_2O (vehicle) were used as controls. MR imaging of mice was conducted using a 7 Tesla MRI (Bruker, USA) under halothane gas anaesthesia before and after injection. TurboRARE-T_2 pulse sequences (TR/TE= 5000 ms/56 ms, Flip angle= 180°, matrix size 256x128) were used for T_2-weighted imaging. The slice thickness was 1 mm with a 1 mm gap, and the field of view (FOV) was 9x 3.5 cm for coronal scanning. To evaluate the heating profile of NIR-activated nanocomposites plus irradiation in tumor region, KB cells xenografted tumor bearing mice were received NIR-activated nanocomposites (0.5 mg Fe/kg) via an intratumoral injection and immediately irradiated with 808 nm NIR laser (2 W/cm^2) for 10 min (692 J/cm^2). The whole process was recorded by thermographic camera (TVS-500 EX, NEX Avio infrared Technologies Co., Ltd.).

Characterization*:* Electron micrographs were obtained using transmission electron microscopes (JEOL 3010 at 300 KV and Philips CM-200 at 200 KV). A UV-Vis spectrophotometer (8452A; Hewlett-Packard Company, Palo Alto, CA) and Hitachi U-4100 UV-vis-NIR spectrophotometer (Hitachi, Ltd., Tokyo, Japan) were used to record absorption characteristics of samples. X-ray photoelectron spectra (XPS) (VG Scientific 210) were recorded using an Mg Kα source (12 kV and 10 mA). The binding energy scale was calibrated to 284.6 eV for the main (C ls) peak. The Fe ions were quantified using an inductively coupled plasma atomic emission spectrometer (ICP-AES, JY138 Spectroanalyzer; Horiba Jobin Yvon, Inc., Edison, NJ). IR spectra were measured using a KBr plate in a Fourier transformation infrared (FTIR) spectrometer (200E; Jasco International Co., Ltd., Tokyo, Japan). The zeta-potential of the NIR-activated nanocomposites dispersed in an aqueous solution (pH = 6) were measured using a Zetasizer analyzer (Malvern Instruments Ltd., Malvern, Worcestershire, UK). The M-H magnetization curves at 300 K were measured for the NIR-activated nanocomposites using a magnetometer (MPMS-7 SQUID; Quantum Design, Inc., San Diego, CA).

References

1. C.-C. Huang, C.-Y. Tsai, H.-S. Sheu, K.-Y. Chuang, C.-H. Su, U-S. Jeng, F.-Y. Cheng, C.-H. Su, H.-Y. Lei, C.-S. Yeh, *ACS Nano* **2011**, *5*, 3905.

2. C.-C. Huang, W. Huang, C.-S. Yeh, *Biomaterials* **2011**, *32*, 556.

3. C.-C. Huang, C.-H. Su, W.-M. Li, T.-Y. Liu, J.-H. Chen, C.-S. Yeh, *Adv. Funct. Mater.* **2009**, *19*, 249–258

4. T. Mosmann, *J. Immunol. Methods* **1983**, *65*, 55-63.

5. a) Y. P. He, Y. M. Miao, C. R. Li, S. Q. Wang, L. Cao, S. S. Xie, G. Z. Yang, B. S. Zou, *Physical Review B*, **2005**, *71*, 125411; b) R. M. Cornell, U. Schwertmann, *The Iron Oxides: Structure, Properties, Reactions, Occurrence and Uses*, **2003**, VCH, Weinheim and New York.

6. B. Zhao, M. E. Itkis, S. Niyogi, H. Hu, J. Zhang, R. C. Haddon, *J. Phys. Chem. B* **2004,** *108,* 8136.

7. a) K. Urbanska, B. Romanowska-Dixon, Z. Matuszak, J. Oszajca, P. Nowak-Sliwinska, G. Stochel, *Acta Biochim. Pol.* **2002**, *43*, 387; b) W. R. Chen, R. L. Adams, R. Carubelli, R. E. Nordquist, *Cancer Lett.* **1997**, *115*, 25.

8. C. J. Orendorff, C. J. Murphy, *J. Phys. Chem. B* **2006,** *110,* 3990.

9. K. Yang, S. Zhang, G. Zhang, X. Sun, S.-T.Lee and Z. Liu, *Nano Lett.,* 2010, **10**, 3318.

10. Roger G. Burns, *Mineralogical Applications of Crystal Field Theory*, 1993, Cambridge University Press; 2 edition.

11. a) M. Yamashita, T. Akai, R. Sawa, J. Abe, M. Matsumura, *J. Non-Cry. Solid* **2008**, *354*, 4534; b) B. Hannoyer, M. Lenglet, J. Dürr, R. Cortes, *J. Non-Cry. Solid* **1992**, *151*, 209; c) R. K. Kulladapu, H. Li, G. L. Smith, J. D. Crum, J.-S. Jeoung, W. H. Poisl, M. C. Weinberg, *J. Non-Cry. Solid* **2003**, *317*, 301.

12. a) A. G. Roca, J. F. Marco, M. d. P. Morales, C. J. Serna, *J. Phys. Chem. C* 2007, *111*, 18577; b) L. M. Bronstein, X. Huang, J. Retrum, A. Schmucker, M. Pink, B. D. Stein, B. Dragnea, *Chem. Mater.* 2007, *19*, 3624.

13. L. H. Dubois, B. R. Zegarski, R. G. Nuzzo, *Langmuir* **1986**, *2***,** 412

14. a) M. Riou-Cavellec, C. Albinet, J.-M. Grenècheb, G. Fèrey, *J. Mater. Chem.* 2001, 11, 3166; b) Y.-W. Li, J.-P. Zhao, L.-F. Wanga, X.-H. Bu, *CrystEngComm* **2011**, *13*, 6002.

15. a) M. Matzapetakis, C. P. Raptopoulou, A. Tsohos, V. Papaefthymiou, N. Moon, A. Salifoglou, *J. Am. Chem. Soc.* **1998,** *120,* 13266; b) I. Shweky, A. Bion, D. P. Goldberg, S. J. Lippard, *Inorg. Chem* **1994**, *33*, 5161.

16. H. Liu, T. Liu, X. Wu, L. Li, L. Tan, D. Chen, and F.Tang, *Adv. Mater.* **2012**, *24*, 755.

17. L. Cheng, K. Yang, Y. Li, X. Zeng, M. Shao, S.-T. Lee, Z. Liu, *Biomaterials* **2012**, *33*, 2215.

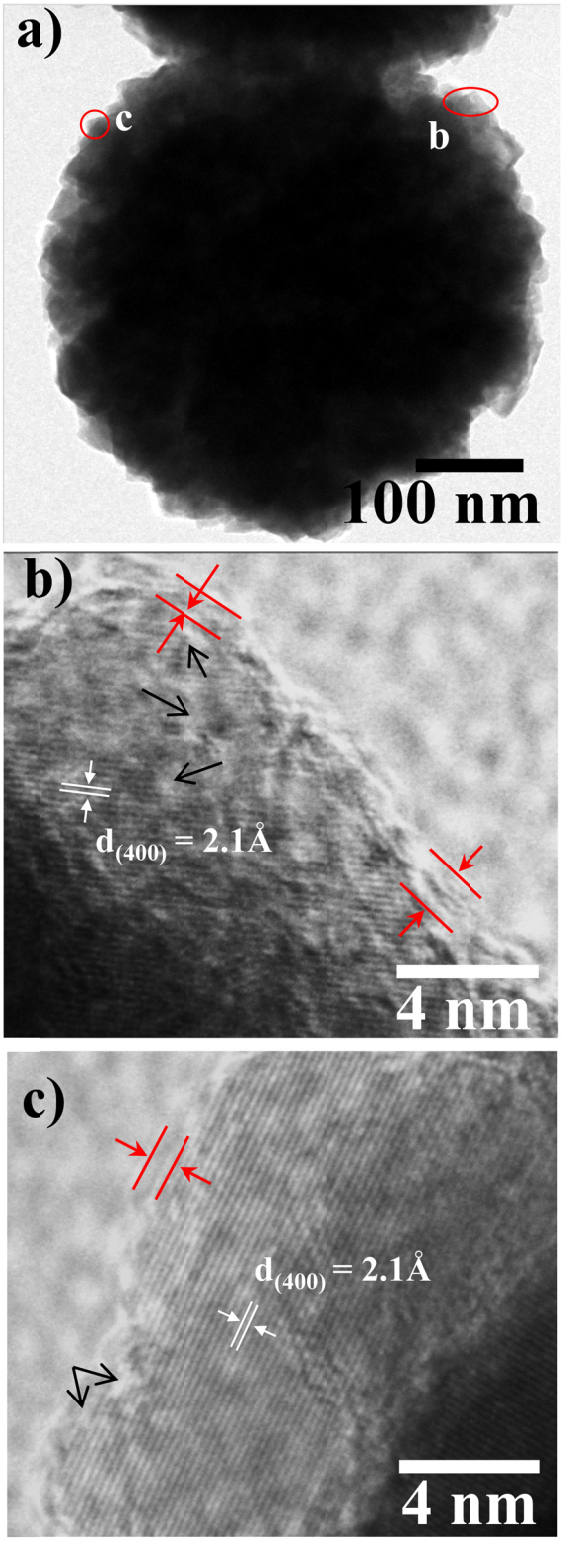

Figure S1. TEM a), and HR-TEM b,c) images for an iron oxide nanostructure after 12 h. The red arrows in b) and c) show amorphous layers. A note by the black arrows shows discontinuous lattice structures with amorphous regions in the surface strucutre of iron oxide nanoproduct.

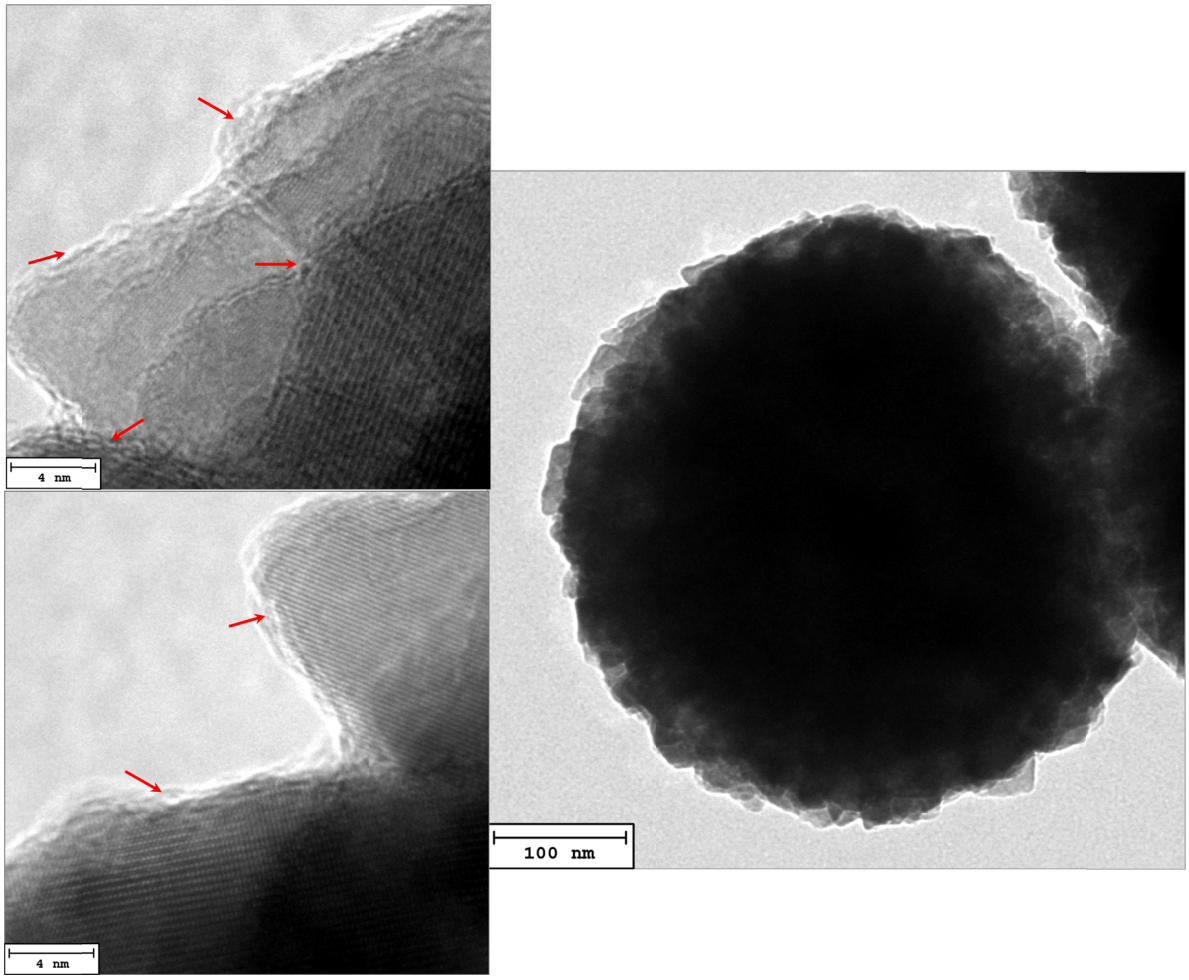

Figure S2. The additional TEM (right) and HRTEM (left) images of another particle for an iron oxide nanostructure after 12 h. The red arrows indicated the amorphous layers covering over the surface of iron oxide nanoproduct.

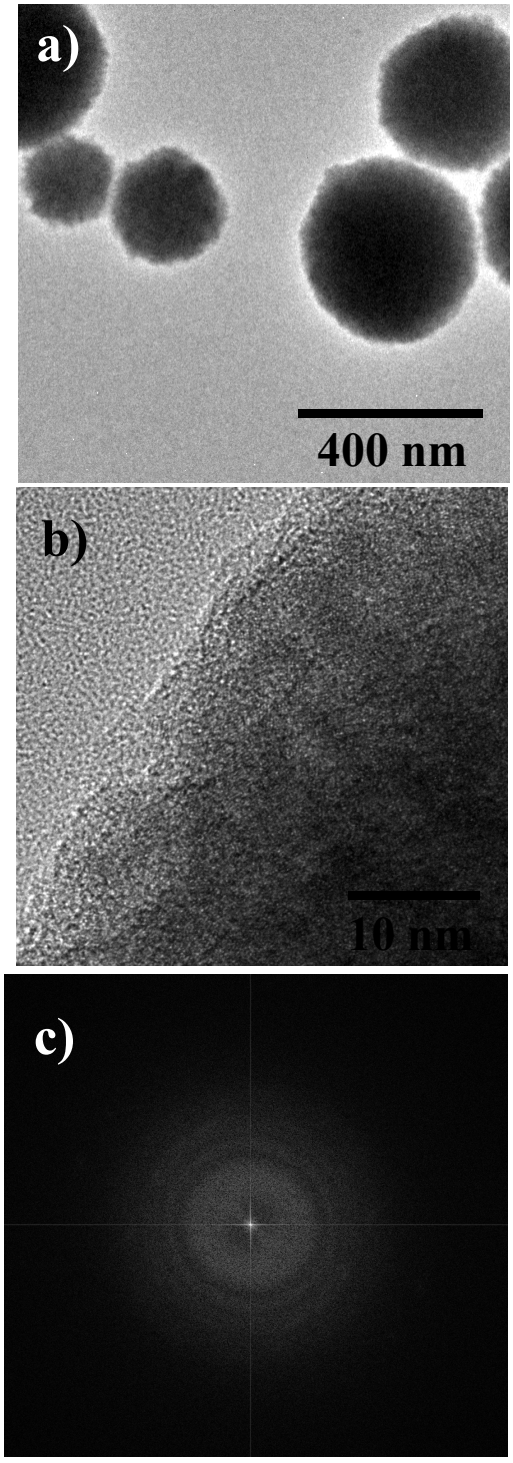

Figure S3. a) TEM image, b) HR-TEM image, and c) fast Fourier transform (FFT) pattern for the preparation of iron oxide nanostructure (after 3 h) with $FeCl_2$+citrate+TMA through hydrothermal reaction at 200 ^oC for 3 h.

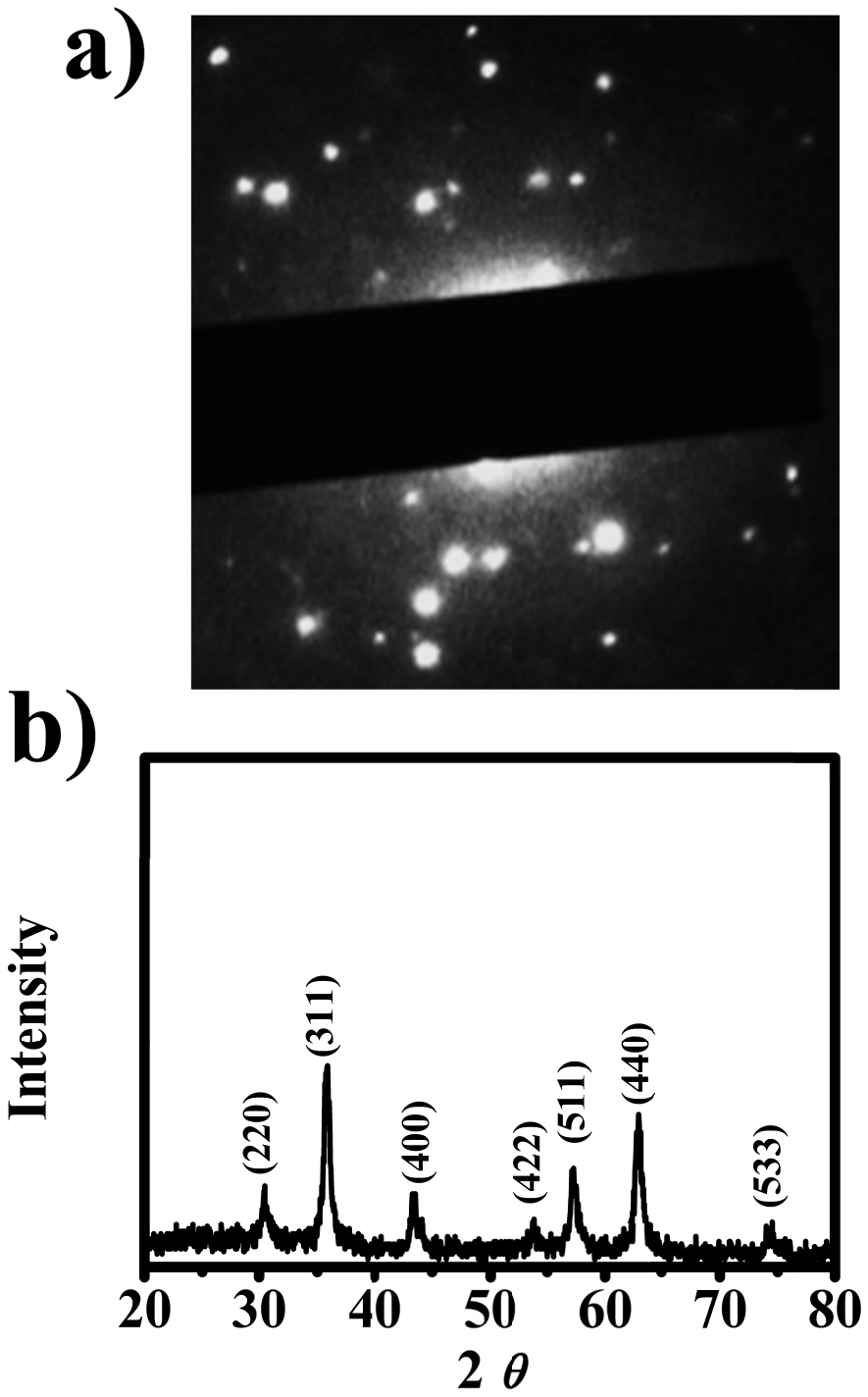

Figure S4. a) ED pattern for a single particle of iron oxide nanostructure after 12 h. b) XRD pattern of iron oxide nanostructure (after 12 h) assigned by JPCDS No. 19-0629.

Using commercial γ-Fe_2O_3 nanopowders as the Fe(III) source, we adapted our ligand-assisted hydrothermal synthesis to the fabrication of visible–NIR-activated α-Fe_2O_3 nanoplates (Figure S5a). The formation of α-Fe_2O_3 nanoplates appeared to occur through the dissolution of γ-Fe_2O_3 (<50 nm) and the subsequent recrystallization of α-Fe_2O_3 (Figure S5b). The α-Fe_2O_3 nanoplates are ~538 nm in diameter and ~46 nm in thickness (Figure S5c). The formation of an amorphous layer around the surfaces of single crystalline nanoplates was noticed and was similar to iron oxide nanostructure after 12 h (Figure S1 and S2), which implies that the surface effect was probably the predominant contributor to the enhancement of the NIR transitions ($^6A_1 \rightarrow {}^4T_1 + {}^4T_2$).[5]

This work is the first reported development of NIR-activated Fe_3O_4 nanostructures (Figure S1 and S2) and α-Fe_2O_3 nanoplates. Based on the Beer–Lambert law, the molar extinction coefficient (ε) at 808 nm for iron oxide nanostructures (after 12 h) was 620 $M^{-1}cm^{-1}$, which is higher than the 382 M^{-1} cm^{-1} calculated for α-Fe_2O_3 nanoplates. The high ε can be explained based on the synergistic effect between Fe(II) d–d transitions and IVCT transitions in the Fe_3O_4 structure. Compared with other NIR-activated materials used in photo-to-thermal conversion, the resulting ε value of NIR-activated Fe_3O_4 nanostructures is greater than 4-120 $M^{-1}cm^{-1}$ in the NIR region of carbon materials (such as carbon black and carbon nanotubes)[6], and it is less than 1.08 x 10^4 M^{-1} cm^{-1} at 778 nm of indocyanine green (NIR dye)[7] and 5.5 x 10^9 M^{-1} cm^{-1} at 845 nm of Au nanorod (aspect ratio 4.5).[8] What should be particularly noted is that carbon-based nanomaterials acting as laser-photosensitizer have been demonstrated for efficiency photothermalysis treatment of a tumor site in vivo.[9]

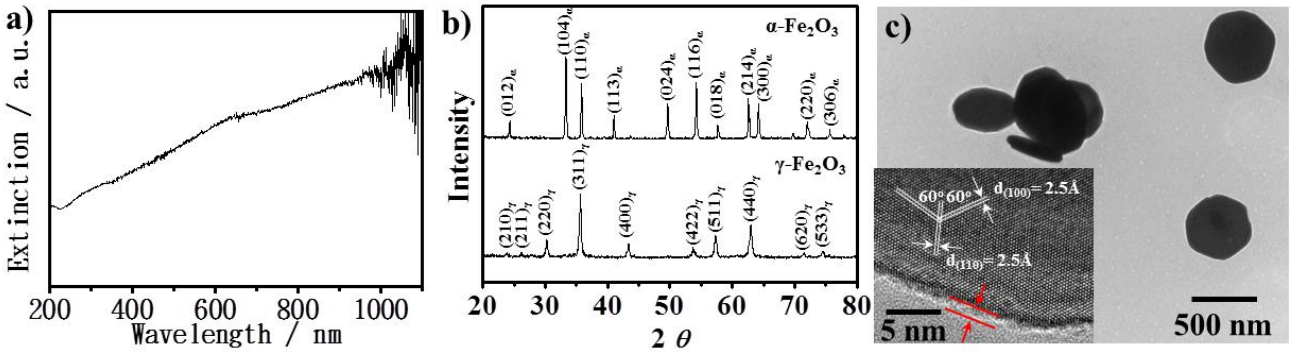

Figure S5. The absorption spectrum a) and XRD measurements b) detected the conversion of commercial γ-Fe_2O_3 nanopowders to α-Fe_2O_3 nanoplates. TEM image c) of α-Fe_2O_3 nanoplates and its corresponding HRTEM image in the inset (the amorphous layer (~ 0.8 nm) is marked with red lines).

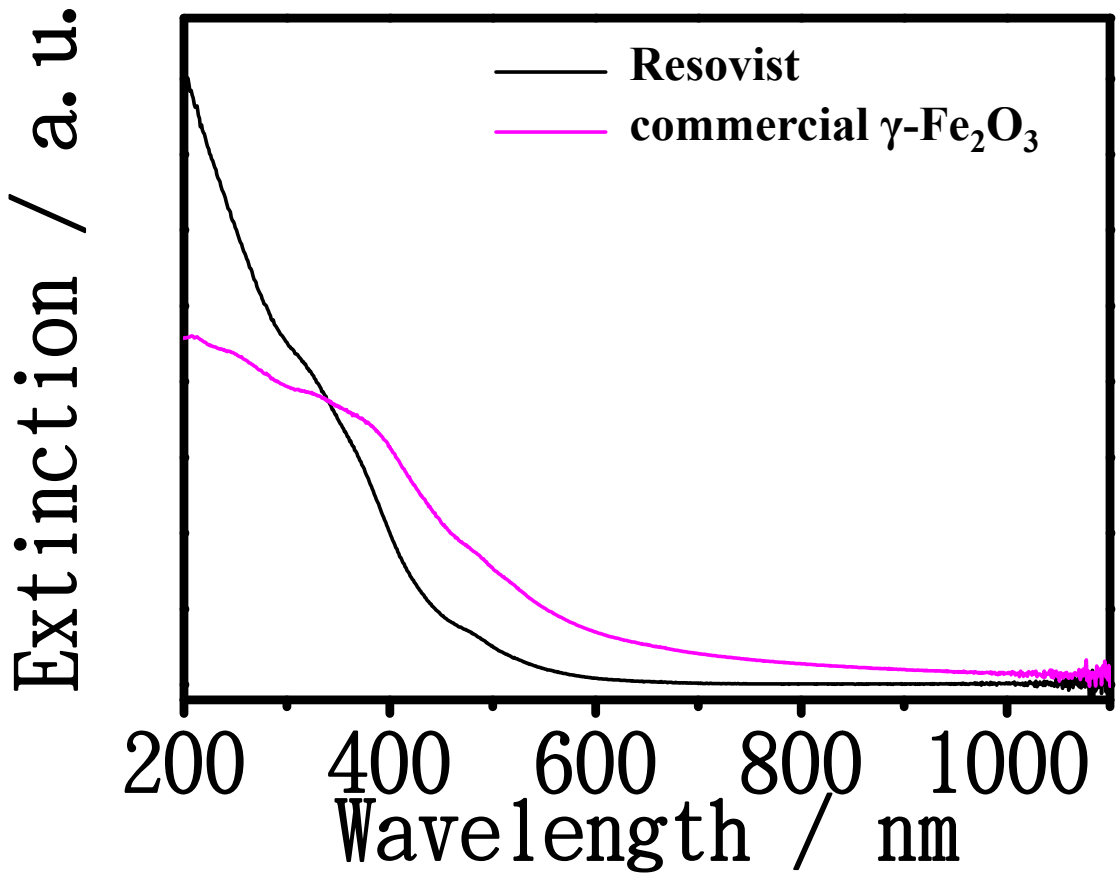

Figure S6. Absorption spectra of clinical Resovist agent and commercial γ -Fe_2O_3 nanopodwers.

An additional observation was that absorption band shifting of as-synthesized iron oxides occurred by adjusting the ratio of $Fe(II)Cl_2$ and $Fe(III)Cl_3$ precursors. Following by XRD measurements, it is observed that a gradual phase conversion from Fe_3O_4 to α-Fe_2O_3 was generated by decreasing the ratio of $Fe(II)Cl_2$ and $Fe(III)Cl_3$ precursors. Therefore, we proposed that the absorption-band shifting might have been caused by both surface and bulk effects (i.e. Fe_3O_4 (surface-ligand inducing NIR absorption) → α-Fe_2O_3 (red color in nature)[5]). Further studies are required and underway.

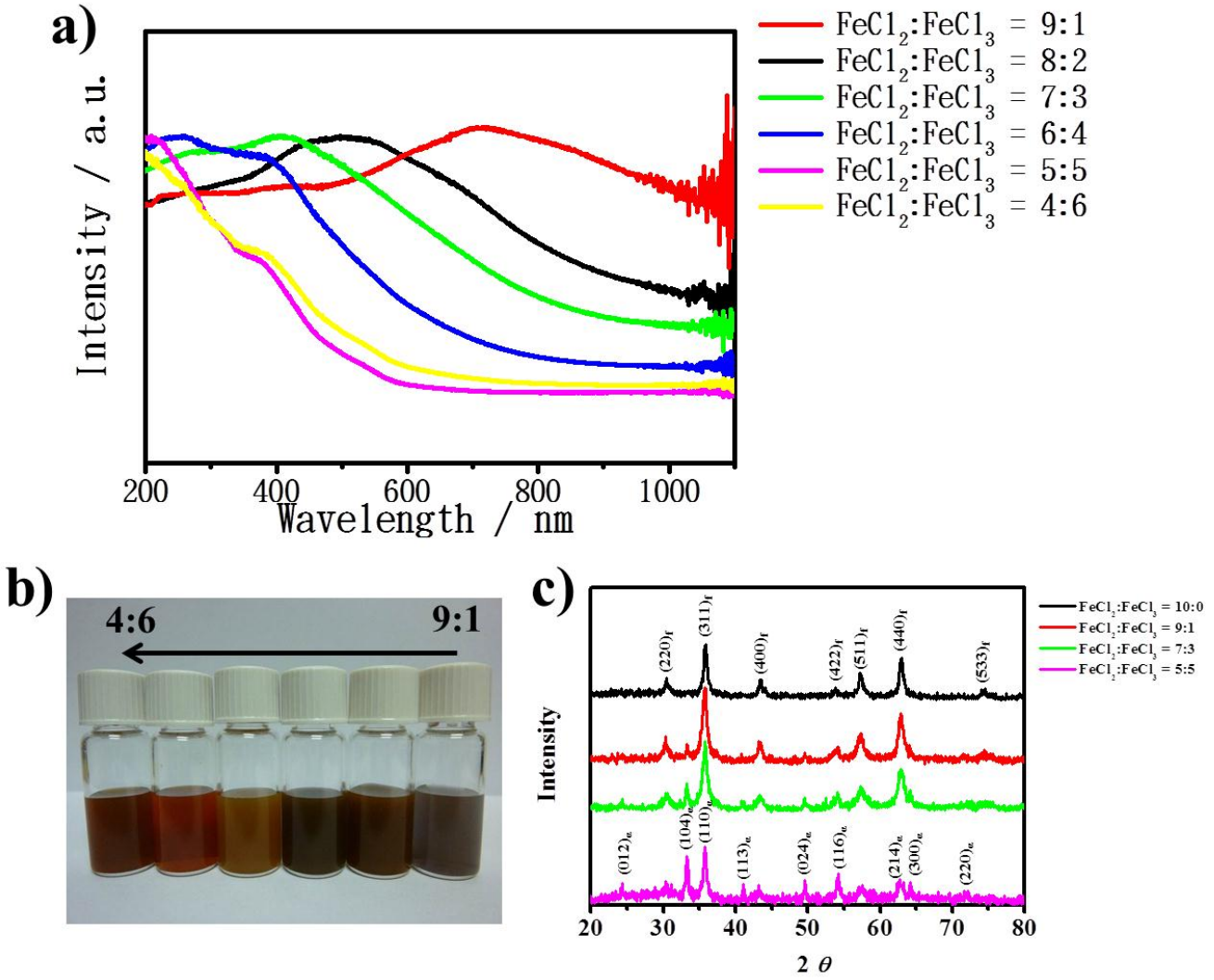

Figure S7. a) Absorption spectra, b) photograph, and c) XRD patterns for the preparation of iron oxide nanostructures with different $FeCl_2$ and $FeCl_3$ precursor ratio including citrate and TMA molecules through hydrothermal reaction at 200 ^oC for 12 h. The subscript labels f and α in Figure S7c indicate fcc-structured Fe_3O_4 and α-Fe_2O_4 crystal structures, respectively.

To better inspect the optical structure of iron oxide nanostructures (after 12 h), another UV–vis–NIR spectrophotometer (Hitachi U-4100) was utilized to detect longer NIR wavelengths of up to 1290 nm and to prevent noise interference in the NIR region. This broadened band can be split via Gaussian deconvolution into respective peaks i-vi (Figure S8) with the following iron d–d transitions:[5,10,11] the ligand-field-related absorption peaks appeared for i at ~ 1200 nm (NIR) by Fe^{2+}; ii at ~ 725 nm, including $^6A_1 \rightarrow {}^4T_1$ (NIR) + $^4T_2$ (visible); iii at ~ 542 nm by pair excitations $2(^6A_1) \rightarrow 2(^4T_1)$ (visible); iv at ~ 415 nm due to the $^6A_1 \rightarrow {}^4E, {}^4A_1 + {}^4T_2$ (visible); and v at ~ 380 nm by $^6A_1 \rightarrow {}^4E$ (UV). The UV band at ~ 260 nm (peak vi) should result from ligand-to-metal charge transfer (LMCT). The contribution in the UV–visible–NIR region must include inter-valence charge-transfer (IVCT) transitions by a process of electron donation from Fe(II) to Fe(III) ions because of the intrinsic Fe_3O_4 structure.[5] In addition, peak overlap was not avoided because of the peaks' broadening features.[11a] However, our assignments (peaks i-vi) were still in approximate agreement with the optical transitions of iron ions reported in the literature; these transitions existed not only in various types of iron oxides[5] but also in iron-containing minerals[10] and Fe-doped soda-lime silicate glasses.[11]

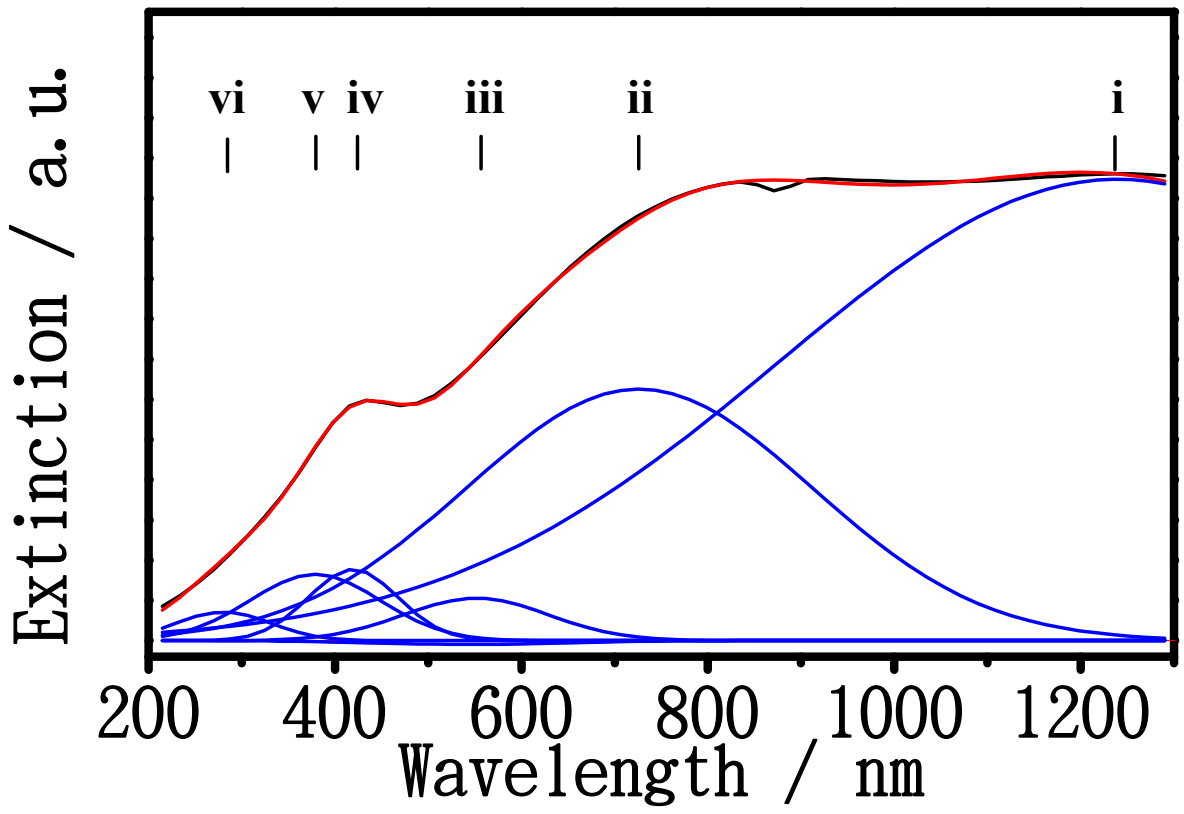

Figure S8. UV-visible-NIR spectrum using Hitachi U-4100 UV-vis-NIR spectrophotometer for iron oxide nanostructures (after 12 h) with contained deconvoluted analysis with Gaussian multiple-peak fitting in accordant with the literature.[5,10,11]

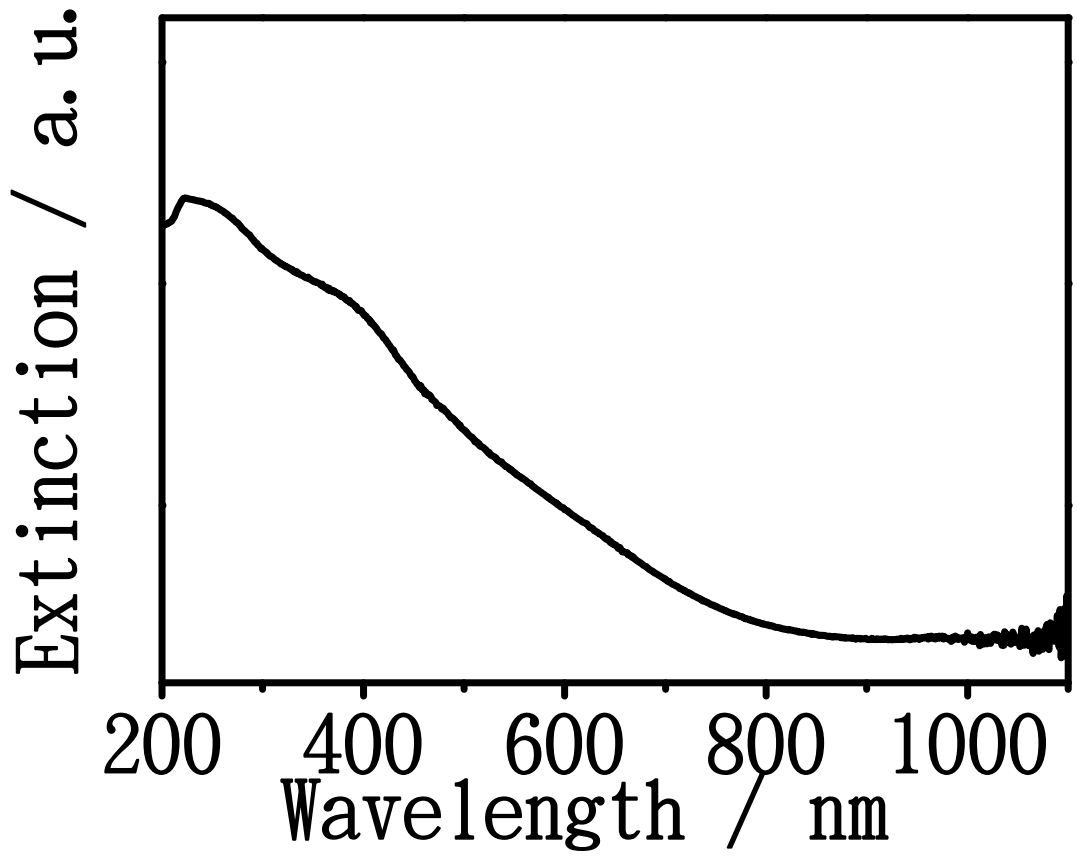

Figure S9. Absorption spectrum for the preparation of iron oxide nanostructures with $FeCl_2$+citrate+ benzoic acid through hydrothermal reaction at 200 ^{o}C for 12 h.

The FT-IR spectra revealed a band at 570 cm^{-1} at 12 h, which is consistent with Fe–O vibrations of the Fe_3O_4 structure.[12a] The absorptions at 1630 (u), 1558 (b), and 1396 cm^{-1} (s) are ascribed to carboxylate groups, in which the labels u and b denote $\nu_{as}(COO)^-$, and s denotes $\nu_s(COO)^-$.[12b] Based on the results of previous investigations, the difference (Δ) between the $\nu_{as}(COO)^-$ and $\nu_s(COO)^-$ positions is correlated with the varying carboxylate coordination states.[13] The peak labeled f at 1730 cm^{-1} is attributed to free –COOH. Following the aforementioned rule,[12b,13] Δ values were estimated to be 243 cm^{-1} (unidentate) according to peak u–s and 162 cm^{-1} (bridging) according to peak b–s. X-ray structural determinations have been used to show that citrate and TMA molecules can octahedrally coordinate to Fe(II) and Fe(III) ions to form Fe–carboxylate complexes with distorted octahedrons.[14,15]

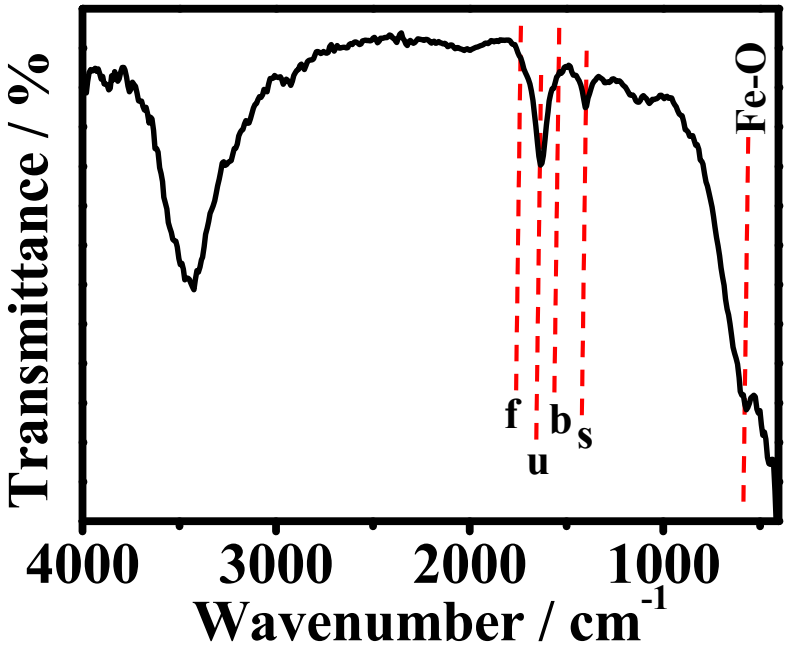

Figure S10. FT-IR measurements for the synthesis of iron oxide nanostructure after 12 h.

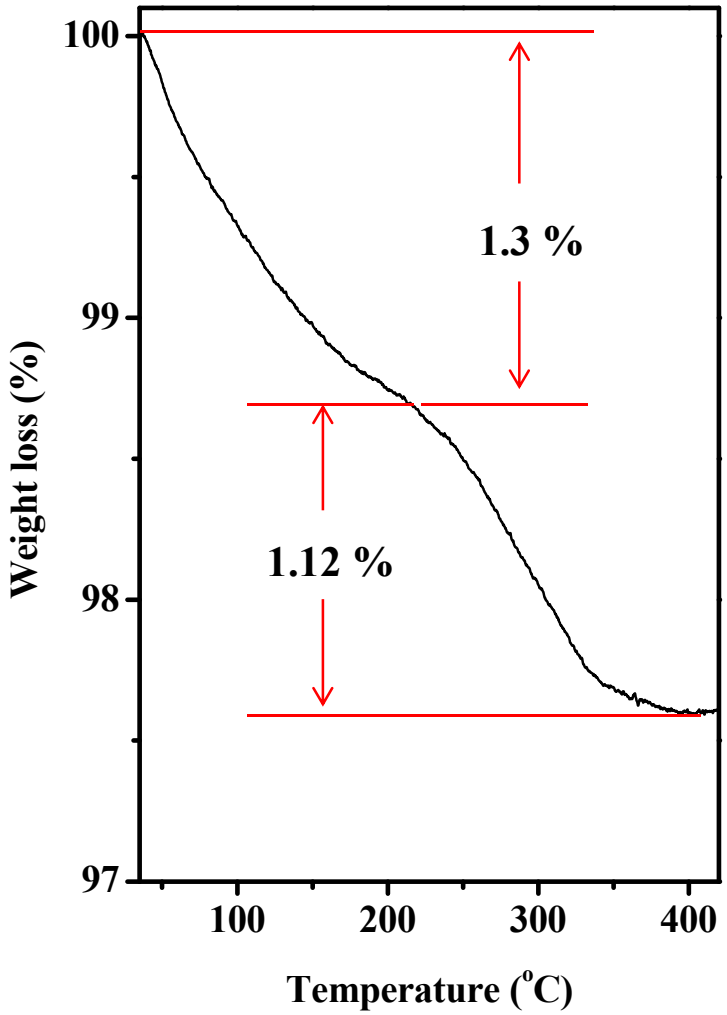

Figure S11. TGA curves of the NIR-activated Fe_3O_4 nanostructures. The initial weight loss of 1.3% is attributed to the loss of adsorbed water at 35–210 °C, while a loss of weight of 1.12% at 210–420 °C is due to the elimination of carboxylate capping molecules.

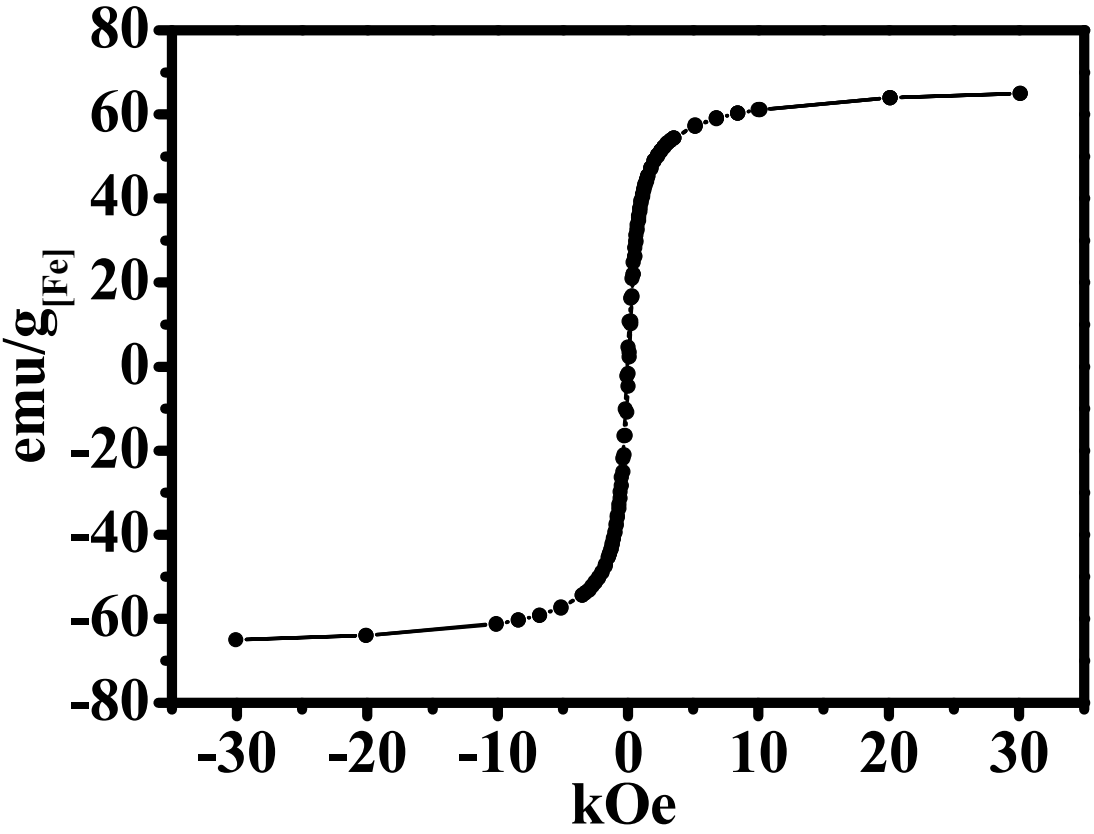

Figure S12. Superconducting quantum interference device (SQUID) measure of iron oxide nanostructure after 12 h at 300 K.

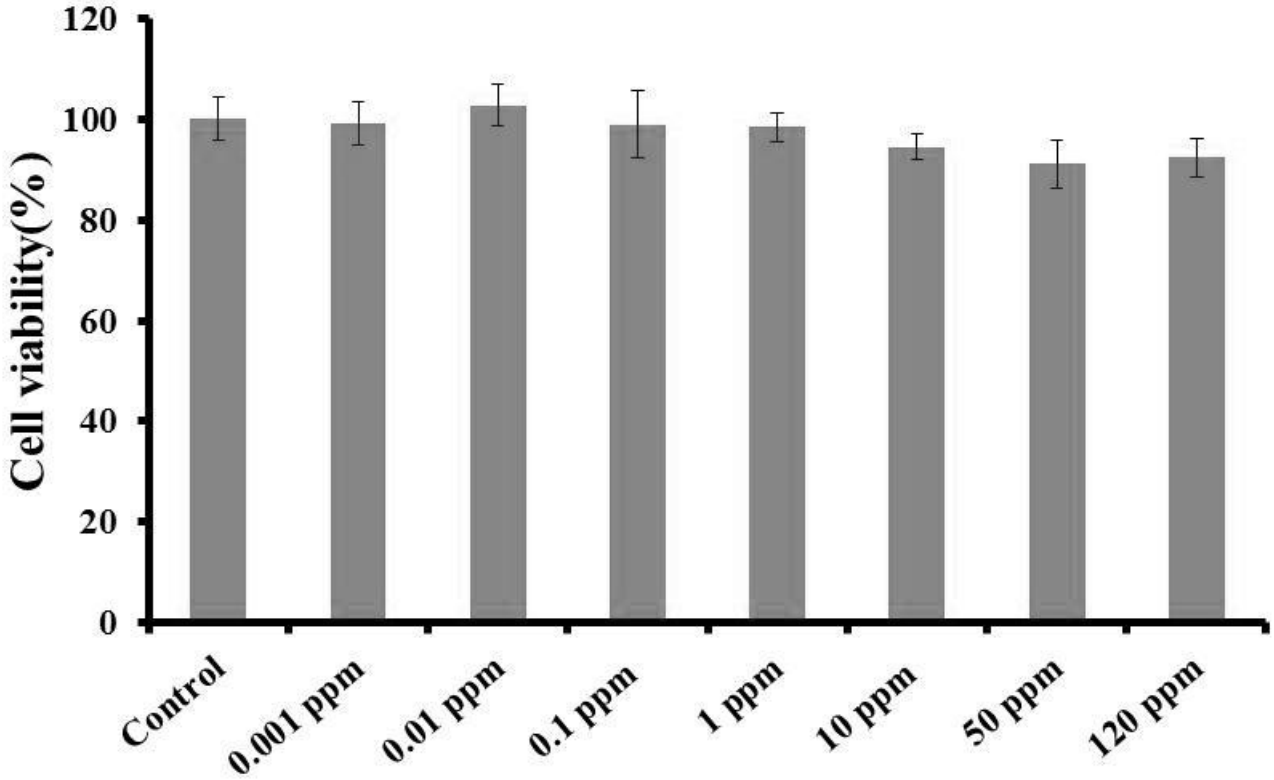

Figure S13. MTT assays of NIR-activated nanocomposites cultured with KB cells for 24 h.

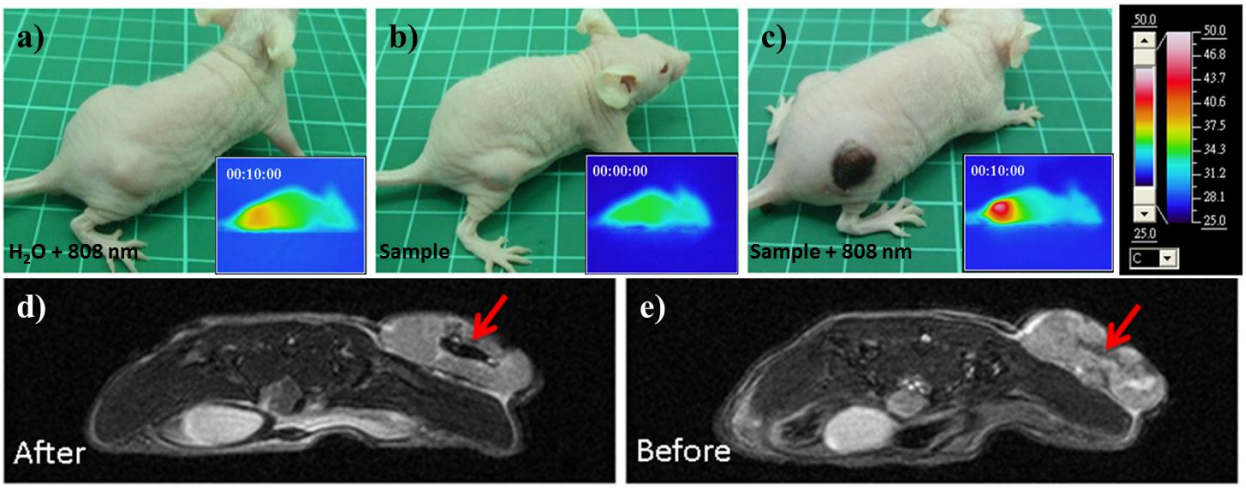

Figure S14. Thermographic imaged mice bearing KB tumors without a) and with c) intratumoral injections of NIR-activated nanocomposites (0.5 mg/kg) after 10 min exposure to 808-nm laser irradiation (2 W/cm^2) compared with a NIR-activated nanocomposite-treated mouse without laser irradiation b). In vivo progressive MRI events. T_2-weighted images of mice bearing KB tumors after d) and before e) intratumoral injections of NIR-activated nanocomposite (0.5 mg/kg). (The red arrows indicate the injection site in tumor region).

Figure S15. Digital image for an observation of a tested mouse with NIR-activated nanocomposite+NIR laser treatment after 4 days postinjection.

In our current synthesis improvment, the preliminary results have demonstrated that the air-aging of $FeCl_2$ powders assisted in the reduction of the particle size to 150-200 nm while maintaining absorption properties that cover the NIR region. Particle size below 200 nm would be feasibility and applicability in the area of nanomedicine via an intravenous injection for biological applications.[16,17]

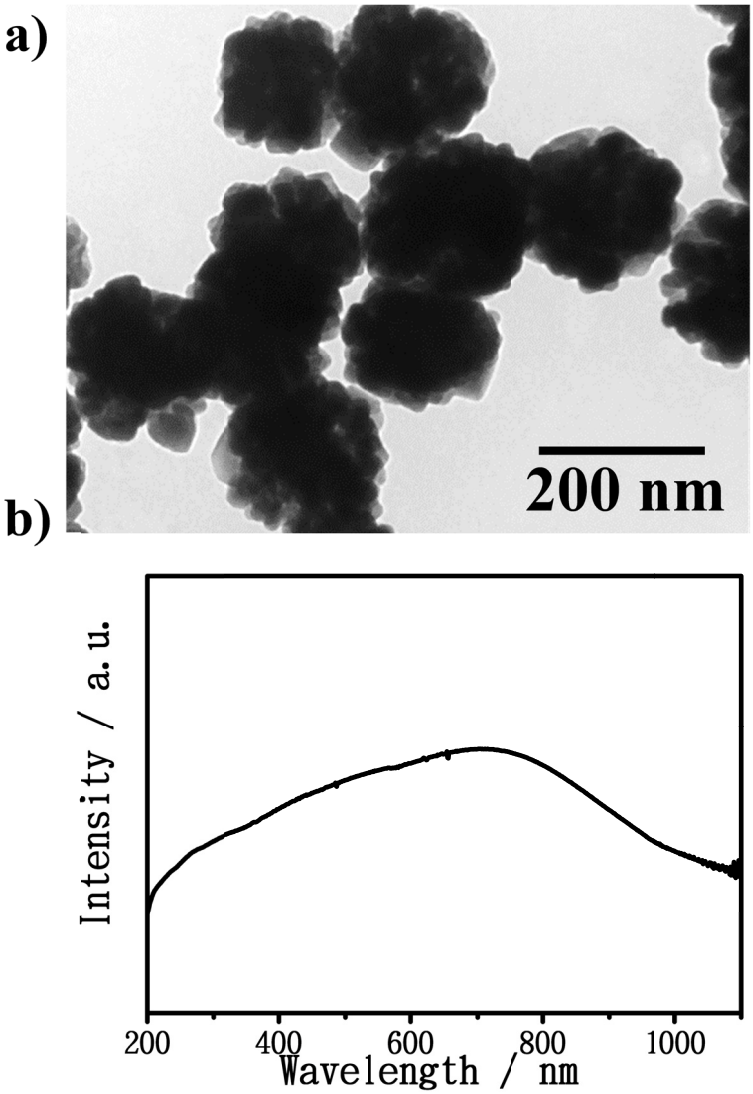

Figure S16. TEM image a) and spectral absorption b) of NIR-activated Fe_3O_4 nanostructures, which were prepared with the air-aging of $FeCl_2$ powders through ligand-assisted hydrothermal reaction.